

ECVC: Exploiting Non-Local Correlations in Multiple Frames for Contextual Video Compression

Wei Jiang, Junru Li, Kai Zhang, Li Zhang[✉]
Bytedance

{jiangwei.lvc, lijunru, zhangkai.video, lizhang.idm}@bytedance.com

Abstract

In Learned Video Compression (LVC), improving inter prediction, such as enhancing temporal context mining and mitigating accumulated errors, is crucial for boosting rate-distortion performance. Existing LVCs mainly focus on mining the temporal movements while neglecting non-local correlations among frames. Additionally, current contextual video compression models use a single reference frame, which is insufficient for handling complex movements. To address these issues, we propose leveraging non-local correlations across multiple frames to enhance temporal priors, significantly boosting rate-distortion performance. To mitigate error accumulation, we introduce a partial cascaded fine-tuning strategy that supports fine-tuning on full-length sequences with constrained computational resources. This method reduces the train-test mismatch in sequence lengths and significantly decreases accumulated errors. Based on the proposed techniques, we present a video compression scheme ECVC. Experiments demonstrate that our ECVC achieves state-of-the-art performance, reducing 10.5% and 11.5% more bit-rates than previous SOTA method DCVC-FM over VTM-13.2 low delay B (LDB) under the intra period (IP) of 32 and -1^1 , respectively.

1. Introduction

Video coding aims to compactly represent the visual signals while maintaining acceptable reconstructed quality. Traditional video coding, such as H.266/VVC [8], is established on the block-based hybrid coding framework, which has been developed for several decades. However, as the performance improvement of traditional codecs approaches a plateau, learned video compression (LVC) has emerged as a promising alternative, attracting significant attention from both academic and industrial fields. The end-to-end optimization [3, 4, 26, 33, 36, 38, 39, 64] of LVCs offers the potential to surpass handcrafted traditional codecs with re-

¹Only one intra frame when compressing a sequence.

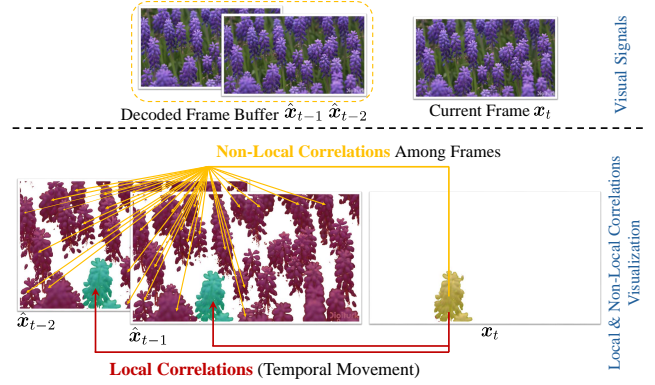


Figure 1. Visualization of local (red lines) correlations \hat{C}^ℓ and non-local (orange lines) correlations \hat{C}^{nl} in sequence ‘‘Honey-Bee’’ in UVG dataset [40]. \hat{C}^{nl} is defined as the distant correlations without explicit movement between the current frame and reference frames. \hat{C}^{nl} is beneficial for temporal context mining due to lower conditional entropy for x_t , formulated as $\mathcal{H}(x_t|\hat{C}^\ell, \hat{C}^{nl}) \leq \mathcal{H}(x_t|\hat{C}^\ell)$, where \mathcal{H} is the Shannon entropy.

dundancy removal.

Early LVCs [15, 19, 30, 32, 33, 35, 42, 43, 46, 61–63] follow the residual coding paradigm, wherein the residuals between the predicted frame (via estimated motion) and the current frame, along with motion information, are compressed. Recently, the conditional coding paradigm [26] has emerged, which leverages temporal information as a prior, enabling a reduction in conditional entropy and offering more flexibility compared to the predefined subtraction used in residual coding. Subsequent research has explored various techniques [2, 10, 11, 14, 17, 24, 27–29, 44, 48, 49, 54, 57, 60, 65] to enhance the performance of conditional coding. Notably, recent DCVC-DC [28] has outperformed the H.266/VVC low delay B (LDB) coding with an intra period (IP) of 32 by exploiting diverse temporal contexts. Additionally, DCVC-FM [29] surpasses the H.266/VVC LDB configuration [8] in long coding chains, particularly when the IP is -1 , by employing temporal feature modulation.

Inter prediction is a long-standing challenge in video coding, aimed at characterizing temporal movements in videos to eliminate temporal redundancies. This temporal information serves as a beneficial contextual prior for current frame coding. Recent advancements in LVC, such as DCVC-DC [28] and DCVC-FM [29], have utilized offset diversity [9] for inter prediction, enabling precise capture of local small-scale movements between frames. However, existing LVC approaches generally overlook non-local correlations. For instance, as illustrated in Figure 1, while the movement of one flower can be accurately estimated, the similarities among different flowers, representing non-local correlations, remain challenging to capture using optical flow [45] / DCN [12]. Moreover, multiple reference frames, a technique commonly adopted in traditional video coding paradigms [21], are not incorporated in DCVC-DC or DCVC-FM. Exploiting non-local correlations across multiple frames could potentially enhance model performance.

To address the limitations on non-local correlations across multiple frames, we propose the **Multiple Frame Non-Local Context Mining (MNLC)** to capture the local and non-local contexts for the t -th frame x_t from two reference frames \hat{x}_{t-1} , \hat{x}_{t-2} , achieving enhanced rate-distortion performance with moderate complexity increases. Specifically, regarding the multiple frames' local correlations, the offset diversity [9] is employed to capture local correlations in \hat{x}_{t-1} . The former motion between \hat{x}_{t-2} and x_{t-1} is reused to exploit local correlations in \hat{x}_{t-2} . To capture non-local correlations, we propose the **Multi-Head Linear Cross Attention (MHLCA)**. Leveraging the flexibility of conditional coding, our model learns non-local correlations through cross-attention between the current mid-feature during transform and multiple temporal priors. The attention mechanism computes similarity among all elements, capturing correlations between distant elements. Additionally, we employ the linear decomposition of vanilla attention [53] to mitigate high complexity. By incorporating both local and non-local priors from multiple frames, our approach significantly enhances the performance.

Error propagation is one of the key issues causing quality degradation in inter frame coding, particularly in scenarios involving long prediction chains (*e.g.*, video conferencing, monitoring scene). The coding distortions in the previously coded frames are sequentially propagated and accumulated to the current frame through inter prediction, significantly damaging the coding efficiency of the current frame. To reduce accumulated prediction errors, DCVC-FM employs propagated feature refreshment, significantly outperforming DCVC-DC. However, the temporal context refreshment in DCVC-FM is not mature enough in achieving consistent performance improvements, especially on videos with fast movements. The primary factor influencing error accumulation is the train-test mismatch in sequence lengths.

Most existing LVCs are trained with only 6 to 7 frames due to the limited computational resources, whereas the testing sequence length may reach to hundreds of frames. Although DCVC-FM attempts to train on long sequences, the vanilla training strategy is still a heavy demand for training resources. To address this issue, we propose the **Partial Cascaded Finetuning Strategy (PCFS)**, enabling finetuning of LVC on full-length sequences, thereby significantly reducing accumulated errors within the computational resources budget.

Based on the proposed techniques, we introduce **Exploiting Non-Local Correlations** in multiple frames for Contextual Video Compression (ECVC), which is established beyond the DCVC-DC. Experiments demonstrate that our ECVC achieves state-of-the-art performance, reducing 7.3% and 10.5% more bit-rates than DCVC-DC and DCVC-FM over VTM-13.2 LDB, respectively under IP 32. Additionally, ECVC reduces 11.5% more bit-rate than DCVC-FM over VTM-13.2 LDB when the IP is -1 . The contributions of this paper are summarized as follows:

- **Enhanced Temporal Priors:** We analyze the potential of exploiting spatial *non-local correlations* in multiple frames and propose a novel multiple-frame non-local context mining module. This module enables the model to aggregate more temporal priors to boost performance. To our knowledge, we are the *first* in the learned video compression community to exploit *non-local correlations* in multiple frames.
- **Mitigated Accumulated Errors:** We address the train-test mismatch in sequence length and propose the novel partial cascaded finetuning strategy, enabling finetuning on unlimited-length sequences with error awareness.
- **Experimental Validation:** The ECVC achieves state-of-the-art performance under IP 32 and IP -1 settings. Specifically, our ECVC reduces 10.5% more bit-rates than DCVC-FM [29] over VTM-13.2 LDB under IP 32. Additionally, ECVC reduces 11.5% more bit-rates than DCVC-FM [29] over VTM-13.2 LDB when the IP is -1 .

2. Related Works

DVC [33] is one of the pioneer learned video compression frameworks, wherein an optical flow net [45] is employed for motion estimation. Then the residuals between predicted frame and original frame are calculated and compressed along with the motion information by neural networks. To further enhance the rate-distortion performance, advanced techniques such scale-space warping [1], adaptive flow coding [18], deformable convolutions (DCN) [12, 19], coarse-to-fine mode prediction [20] and pixel-to-feature motion compensation [50] are investigated, leading to the improvement of the prediction accuracy.

Recently, Li *et al.* [26] proposed the conditional coding framework DCVC, wherein the temporal information

serves as the context for current frame coding instead of explicitly residual coding. In this way, the network learns the correlations between temporal context and current frame automatically. The conditional coding is more flexible and thus breaks the performance bound of residual coding. DCVC-TCM [48] employs the multi-scale temporal contexts and temporal propagation mechanism to exploit more temporal priors. Li *et al.* [27] further enhances the performance via advanced dual spatial contexts for entropy modeling. In DCVC-DC [28], a hierarchical quality structure is employed to alleviate the error propagation. In DCVC-FM [29], the temporal propagated contexts are periodically refreshed to further enhance the performance with a long prediction chain (*e.g.* one intra frame setting).

However, existing DCVC series only consider the local correlations in inter prediction. The non-adjacent correlations are ignored, which limits the potential for performance improvement of LVCs. In addition, considering that videos contain complex scenes and motions, such as fast movements [13], affine motions [66], and occlusion [21], one single reference frame may not effectively capture such complicated scenario. Multiple reference frames can provide richer motion information. Moreover, although DCVC-FM achieves remarkable performance under a long prediction chain, the temporal context refreshment in DCVC-FM is not mature enough to achieve consistent performance improvements, especially on videos with fast movements. There is room for further reducing the error propagation.

3. Method

3.1. Overview of ECVC

The proposed ECVC builds upon the DCVC-DC [28], but focuses more on exploiting non-local correlations in multiple frames. The architecture of ECVC is presented in Figure 2 and Figure 3. The method processes the t -th frame x_t by firstly converting the propagated features \hat{F}_t, \hat{F}_{t-1} into multi-scale features $\hat{F}_t^i, \hat{F}_{t-1}^i \in \mathbb{R}^{\frac{H}{2^i} \times \frac{W}{2^i} \times d_f^i}, 0 \leq i \leq 2$, targeting at the coding of mid-feature $y_t^i \in \mathbb{R}^{\frac{H}{2^i} \times \frac{W}{2^i} \times d_e^i}$, where H, W are the height and width. d_f^i, d_e^i denote channel numbers. A key innovation is the Multiple Frame Non-Local Context Mining, which leverages multiple reference frames to extract local and non-local contexts. For local contexts $\hat{C}_{t-1 \rightarrow t}^{\ell, i}$ and $\hat{C}_{t-2 \rightarrow t}^{\ell, i}$, we use motion vectors \hat{v}_t and \hat{v}_{t-1} to capture local contexts from the multi-scale features \hat{F}_t^i and \hat{F}_{t-1}^i via the offset diversity and proposed multi-scale refinement module, yielding priors from *two* reference frames. For non-local contexts, the Multi-Head Linear Cross Attention is proposed to capture non-local contexts $\hat{C}_{t-1 \rightarrow t}^{nl, i}$ and $\hat{C}_{t-2 \rightarrow t}^{nl, i}$ among $y_t^i, \hat{F}_t^i, \hat{F}_{t-1}^i$. Those local and non-local contexts are then used for conditional coding of y_t^i . The decoding process mirrors the encoding process but uses \hat{y}_t^i as input instead of y_t^i . Besides, a Partial

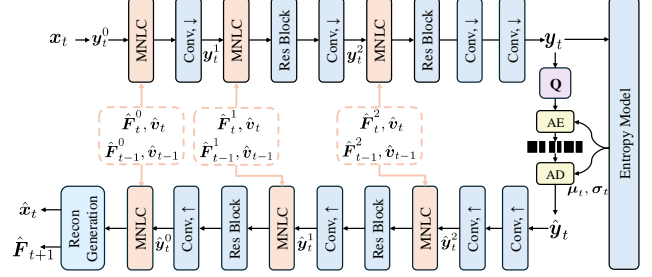


Figure 2. Illustration of contextual encoder and decoder. x, \hat{x} are input frame and reconstructed frame. \hat{F}_{t+1} is the propagated feature for coding x_{t+1} . \hat{v}_t, \hat{v}_{t-1} are motion vectors. $\{y_t^0, y_t^1, y_t^2\}, \{\hat{y}_t^0, \hat{y}_t^1, \hat{y}_t^2\}$ are mid-features during encoding and decoding. “Res Block” and “Recon Generation” are adopted from DCVC-DC. “Q” is quantization. “AE” denotes arithmetic encoding and “AD” denotes arithmetic decoding. μ_t and σ_t are estimated means and scales of \hat{y}_t by the entropy model for AE/AD.

Cascaded Finetuning Strategy (PCFS) is proposed to further mitigate error accumulation, as depicted in Figure 4.

3.2. Exploiting Non-Local Correlations

As illustrated in Figure 1, there are both local and non-local correlations between the current frame and reference frames. Existing methods mainly focus on capturing local correlations (*i.e.* temporal movement). It is desirable to capture both local and non-local correlations (*i.e.* similar regions without explicit movement) to boost the performance. In addition, considering that videos contain complex scenes and motions [21, 66], using a single reference frame may not effectively capture complicated scenarios. Multiple reference frames can provide richer motion information. To tackle these issues, we propose the Multiple Frame Non-Local Context Mining, where two reference frames are employed on account of maintaining the complexity. The process of conditionally coding y_t^i is employed as an example and depicted in Figure 3. Specifically, the offset diversity is adopted and extended for two reference frames. \hat{F}_t^i is first warped by decoded motion vector \hat{v}_t to \bar{F}_t^i and then refined by offset diversity to $\hat{C}_{t-1 \rightarrow t}^{\ell, i}$. The process is:

$$\hat{C}_{t-1 \rightarrow t}^{\ell, i} = \text{OffsetDiversity}(\text{Warp}(\hat{F}_t^i, \hat{v}_t), \hat{v}_t). \quad (1)$$

To capture additional local contexts from \hat{F}_{t-1}^i , the previous local context $\hat{C}_{t-2 \rightarrow t-1}^{\ell, i}$ is reused to avoid *additional motion bits*. $\hat{C}_{t-2 \rightarrow t-1}^{\ell, i}$ is firstly warped by \hat{v}_t and then refined to local context $\hat{C}_{t-2 \rightarrow t}^{\ell, i}$ by a multi-scale refinement module which can be formulated as:

$$\hat{C}_{t-2 \rightarrow t}^{\ell, i} = \text{MultiScaleRefine}(\text{Warp}(\hat{C}_{t-2 \rightarrow t-1}^{\ell, i}, \hat{v}_t)). \quad (2)$$

To capture non-local correlations, it is necessary to compare *all* elements, which implies the receptive field should

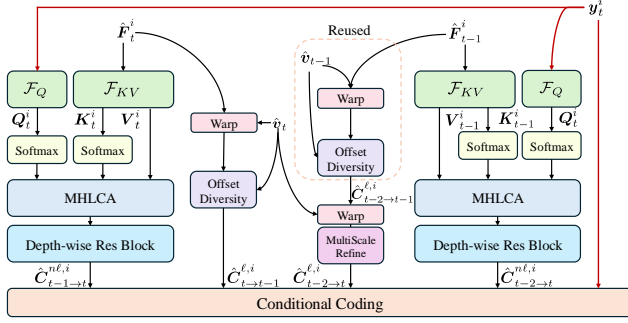


Figure 3. Proposed Multiple Frame Non-Local Context Mining (MNL) for conditional coding of the y_t^i .

be large enough. The offset diversity is not sufficient due to its limited kernel sizes of convolutions. The necessity of large receptive fields inspires us to employ attention mechanisms. Thanks to the flexible conditional coding paradigm, the network itself is able to learn the non-local correlations by cross attention between the current feature and given temporal contexts. For simplicity, we omit the Depth-wise Res Block in Figure 3. The non-local contexts $\hat{C}_{t-1 \rightarrow t}^{nl,i}$, $\hat{C}_{t-2 \rightarrow t}^{nl,i}$ from \hat{F}_t^i , \hat{F}_{t-1}^i for y_t^i can be captured by,

$$\begin{aligned} \hat{C}_{t-1 \rightarrow t}^{nl,i} &= \underbrace{\text{Softmax}(\underbrace{Q_t^i (K_t^i)^\top}_{\mathcal{O}(H^2 W^2 d)} V_t^i)}_{\mathcal{O}(H^2 W^2 d + H^2 W^2 d)} \\ \hat{C}_{t-2 \rightarrow t}^{nl,i} &= \text{Softmax}(Q_t^i (K_{t-1}^i)^\top V_{t-1}^i), \end{aligned} \quad (3)$$

where $Q_t^i = \mathcal{F}_Q(y_t^i)$, $K_t^i, V_t^i = \mathcal{F}_{KV}(\hat{F}_t^i)$, $K_{t-1}^i, V_{t-1}^i = \mathcal{F}_{KV}(\hat{F}_{t-1}^i)$, $Q_t^i, K_t^i, V_t^i, K_{t-1}^i, V_{t-1}^i \in \mathbb{R}^{\frac{H}{2^i} \times \frac{W}{2^i} \times d}$, d is the output channel number of embedding. $\mathcal{F}_Q, \mathcal{F}_{KV}$ are the embedding layer for queries, keys, and values. However, the resolutions of input sequences could be 2K or 4K, which means the complexity could not be too high. The complexity of Equation (3) is $\mathcal{O}(H^2 W^2 d)$. To make the exploiting of non-local correlations possible, it is important to reduce the complexity. The key of Equation (3) is the *non-negativity* of the attention map. Therefore the generalized attention mechanism could be $\text{Similarity}(Q_t^i, (K_t^i)^\top) V$. Inspired by recent advancements in linear attention [16, 22, 23, 25, 47], it is promising to apply a non-negative projection functions ψ, ϕ to Q_t^i and K_t^i to make $\psi(Q_t^i) \phi(K_t^i) \geq 0$. The other key of Equation (3) is the normalized value, which makes it like the probabilities. Inspired by the two factors, we employ the **Multi-Head Linear Cross Attention** (MHLCA), which applies two independent softmax operations on row and column [47] on queries and keys according to Theorem 1.

Theorem 1. Like standard vanilla attention, each row of the implicit similarity matrix $\text{Softmax}_2(Q) \text{Softmax}_1(K)^\top$

sums to 1, representing a normalized attention distribution across all positions.

Proof. Evidently, each row of the similarity matrix in standard attention sums to 1. Let $\text{Softmax}_2(Q) = \mathcal{Q} \in \mathbb{R}^{L \times C}$, $\text{Softmax}_1(K)^\top = \mathcal{K}^\top \in \mathbb{R}^{C \times L}$, where

$$\mathcal{Q} = \begin{bmatrix} q_{1,1} & \cdots & q_{1,C} \\ \vdots & \ddots & \vdots \\ q_{L,1} & \cdots & q_{L,C} \end{bmatrix}, \mathcal{K}^\top = \begin{bmatrix} k_{1,1} & \cdots & k_{1,L} \\ \vdots & \ddots & \vdots \\ k_{C,1} & \cdots & k_{C,L} \end{bmatrix}. \quad (4)$$

Due to the properties of the softmax operation, we have $\sum_{i=1}^C q_{j,i} = 1, 1 \leq j \leq L$; $\sum_{i=1}^L k_{j,i} = 1, 1 \leq j \leq C$.

$$\mathcal{Q} \mathcal{K}^\top = \begin{bmatrix} \sum_{i=1}^C q_{1,i} k_{i,1} & \cdots & \sum_{i=1}^C q_{1,i} k_{i,L} \\ \vdots & \ddots & \vdots \\ \sum_{i=1}^C q_{L,i} k_{i,1} & \cdots & \sum_{i=1}^C q_{L,i} k_{i,L} \end{bmatrix}. \quad (5)$$

Consider the sum of the ℓ -th row ($1 \leq \ell \leq L$):

$$\begin{aligned} \text{Sum}_\ell &= \sum_{i=1}^C q_{\ell,i} k_{i,1} + \sum_{i=1}^C q_{\ell,i} k_{i,2} + \cdots + \sum_{i=1}^C q_{\ell,i} k_{i,L} \\ &= (q_{\ell,1} k_{1,1} + q_{\ell,2} k_{2,1} + \cdots + q_{\ell,C} k_{C,1}) \\ &\quad + \cdots \\ &\quad + (q_{\ell,1} k_{1,L} + q_{\ell,2} k_{2,L} + \cdots + q_{\ell,C} k_{C,L}) \\ &= q_{\ell,1} \underbrace{\sum_{i=1}^L k_{1,i}}_1 + \cdots + q_{\ell,C} \underbrace{\sum_{i=1}^L k_{C,i}}_1 = \sum_{i=1}^C q_{\ell,i} = 1. \end{aligned} \quad (6)$$

Thus, each row of the similarity matrix sums to 1, completing the proof. \square

The softmax-based non-linear projection of queries and keys makes it able to compute the product of keys and values first, resulting in linear complexity $\mathcal{O}(HWd^2)$. The non-local contexts $\hat{C}_{t-1 \rightarrow t}^{nl,i}$, $\hat{C}_{t-2 \rightarrow t}^{nl,i}$ can be learned *linearly* by

$$\begin{aligned} \hat{C}_{t-1 \rightarrow t}^{nl,i} &= \text{Softmax}_2(Q_t^i) \underbrace{(\text{Softmax}_1(K_t^i)^\top V_t^i)}_{\mathcal{O}(HWd^2)} \\ &\quad \underbrace{\mathcal{O}(HWd^2 + HWd^2)} \\ \hat{C}_{t-2 \rightarrow t}^{nl,i} &= \text{Softmax}_2(Q_t^i) (\text{Softmax}_1(K_{t-1}^i)^\top V_{t-1}^i). \end{aligned} \quad (7)$$

The captured local contexts $\hat{C}_{t-1 \rightarrow t}^{\ell,i}$, $\hat{C}_{t-2 \rightarrow t}^{\ell,i}$, and non-local contexts $\hat{C}_{t-1 \rightarrow t}^{nl,i}$, $\hat{C}_{t-2 \rightarrow t}^{nl,i}$ are employed as priors to conditional coding y_t^i . The complexity of Equation (7) is $\frac{d}{HW}$ of that of Equation (3). If $H = 1920$, $W = 1080$, $d = 48$, the complexity of Equation (7) is only 0.002% of that of Equation (3). The process of decoding is similar to that of encoding, except that the input y_t^i is replaced with \hat{y}_t^i .

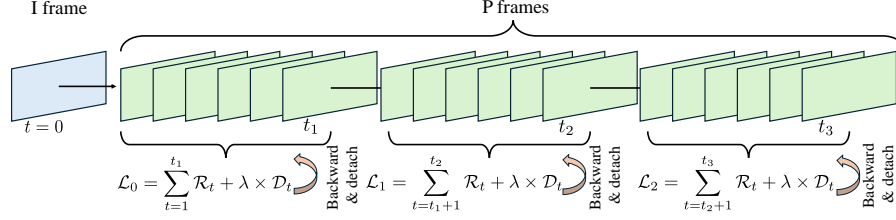


Figure 4. Proposed Partial Cascaded Finetuning Strategy (PCFS). The I frame model is frozen during finetuning.

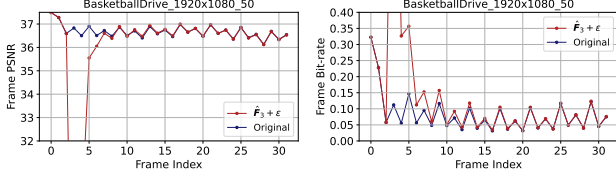


Figure 5. PSNR / Bpp changes of DCVC-DC [28] when the propagated feature \hat{F}_3 is with random Gaussian Noise $\epsilon \sim \mathcal{N}(0, 1)$.

3.3. Enhanced Long Coding Chain Adaptation

In low delay scenarios (*e.g.*, video conferencing, monitoring scene), one sequence may contain hundreds of frames with only one initial intra frame under long coding chains. For enhanced long coding chain adaptation, it is desirable to have the model experience long coding chains during training. However, most existing LVCs [27, 31, 33, 48] are trained using a maximum of 6 – 7 frames, resulting in a significant train-test mismatch in terms of intra period. This discrepancy leads to the accumulation of substantial errors. Addressing the challenge of reducing accumulated errors within limited computational resources remains a critical area of investigation. Conventionally, LVC models are trained using a cascaded loss function [34, 48]:

$$\mathcal{L} = \sum_{t=1}^T \mathcal{R}_t + \lambda \times \mathcal{D}_t, \quad (8)$$

where T is the length of frames used for training, \mathcal{R}_t is the frame bit-rate, \mathcal{D}_t is the frame distortion. Increasing the frame count during training, however, results in escalated GPU memory consumption, posing a substantial computational burden.

To mitigate above issue, we propose a partial cascaded finetuning strategy (PCFS) following initial training on 6 frames. *In low-delay scenarios, neighboring frames have a greater impact on the current frame's coding than distant frames.* As illustrated in Figure 5, if the propagated feature \hat{F}_3 is with Gaussian noise, the coding performances of Frame 3 ~ 13 are significantly influenced, especially of the bit-rate while the coding performances of frame 13 ~ 32 are less affected. Thus, our approach involves

partitioning the finetuning sequences into several groups. When a group is fed into our ECVC, the associated loss and the gradients are computed to update the model. The PCFS process is illustrated in Figure 4. The process is formulated as:

$$\theta_{j+1} = \theta_j - \alpha \nabla \sum_{t=t_j+1}^{t_{j+1}} \mathcal{R}_t + \lambda \mathcal{D}_t, \quad (9)$$

where θ is the model weight, $j \in \mathbb{N}$ is the group index, α is the learning rate and $t_0 = 0$. Empirically, this straightforward method yields effective results, despite the gradient of the first frame in each group not propagating to its previous frames. A potential extension could involve a shifted-window mechanism to enhance gradient propagation, although our results indicate no performance improvement over the original PCFS. The PCFS alleviates error accumulation due to two aspects: (1) fine-tuning on longer sequences reduces the mismatch between training and testing; (2) the calculation of the loss within each group is cascaded, which makes the error propagation within the group aware during fine-tuning owing to the effect of the gradients.

4. Experiments

4.1. Experimental Setup

The proposed ECVC is implemented with Pytorch 2.2.2 [41] and trained with Vimeo-90K train split [59] and BVI-DVC dataset [37] with 4 Tesla A100-80G GPUs. Following the DCVC series [27–29, 48], we apply the multi-stage training [48] on Vimeo-90K. The ECVC is further finetuned on BVI-DVC with the proposed partial cascaded training strategy. The sequences are randomly cropped to 256×256 patches and the batch size is 4 during training and finetuning. In the finetuning stage, 55 frames are involved and divided into 3 groups and the learning rate is 10^{-6} . The loss function is $\mathcal{L} = \mathcal{R} + \lambda \times \mathcal{D}$, where \mathcal{R} is the bit-rate and \mathcal{D} is the distortion. The λ is set to {85, 170, 380, 840} for different bit-rates when ECVC is optimized for MSE and the λ is set to {7.68, 15.36, 30.72, 61.44} when ECVC is optimized for MS-SSIM [56]. We employ the intra frame codec of DCVC-DC [29] for intra frame coding.

Following existing literature [26–29, 36, 48, 49], ECVC is evaluated on HEVC datasets [7], including class B, C,

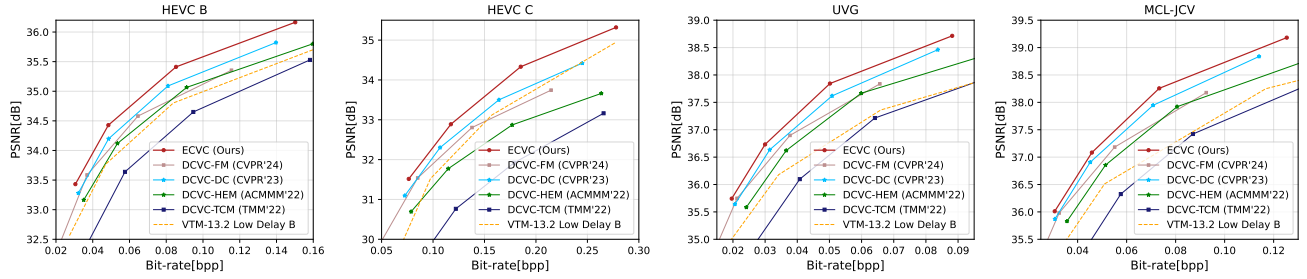


Figure 6. Rate-Distortion curves on HEVC B, HEVC C, UVG and MCL-JCV dataset. **The intra period is 32 with 96 frames.**

Method	Venue	BD-Rate (%) w.r.t. VTM-13.2 LDB [8]						
		HEVC B	HEVC C	HEVC D	HEVC E	UVG [40]	MCL-JCV [55]	Average
DCVC-TCM [48]	TMM'22	+28.5	+60.5	+27.8	+67.3	+17.1	+30.6	+38.6
DCVC-HEM [27]	ACMMM'22	-5.1	+15.0	-8.9	+7.1	-18.2	-6.4	-2.8
DCVC-DC [28]	CVPR'23	-17.4	-9.8	-29.0	-26.0	-30.0	-20.0	-22.0
DCVC-FM [29]	CVPR'24	-12.5	-10.3	-26.5	-26.9	-24.0	-12.7	-18.8
ECVC	Ours	-28.3	-19.6	-36.7	-27.1	-37.6	-26.3	-29.3

¹ The quality indexes of DCVC-FM are set to match the bit-rate range of DCVC-DC.

Table 1. BD-Rate (%) [5] comparison for PSNR (dB). The anchor is **VTM-13.2 LDB**. **The Intra Period is 32 with 96 frames.**

D, E, UVG [40] and MCL-JCV [55]. To fully demonstrate the superiority of the ECVC, we compare the ECVC with DCVC-TCM [48], DCVC-HEM [27], DCVC-DC [28], and DCVC-FM [29]. The testing scenarios are low delay with IP 32 and IP -1 [6]. The distortion metric is PSNR and MS-SSIM [56] in RGB color format.

4.2. Comparisons with Previous SOTA Methods

Under IP 32 The results under IP 32 are presented in Table 1, Table 2 and Figure 12. Our ECVC outperforms DCVC-DC and DCVC-FM on all datasets. Specifically, the ECVC achieves an average of 29.3% bit-rate saving over the VTM-13.2. The bit-rate savings of DCVC-DC and DCVC-FM are 22% and 18.8%, respectively. The performance improvements over DCVC-DC demonstrate the superiority of the proposed techniques. In addition, regarding the MS-SSIM optimized models, ECVC achieves an average of 56.6% bit-rate saving over the VTM-13.2. The proposed ECVC outperforms the DCVC-DC by reducing 3.7% more bit-rate.

Under IP -1 The results under IP -1 are presented in Table 3, Table 4 and Figure 13. Following DCVC-FM [29], the performance under IP -1 is evaluated on 96 frames and *all* frames. When evaluated on 96 frames, our ECVC reduces 11.1% more bit-rate over VTM-13.2 compared to DCVC-FM. When evaluated on *all* frames, our ECVC reduces 11.5% more bit-rate over VTM-13.2 compared to DCVC-FM. The significant performance improvement of our ECVC over DCVC-DC and DCVC-FM demonstrates

the effectiveness of the proposed techniques.

Subjective quality comparison The subjective quality comparison is presented in Figure 8. Compared with DCVC-FM, the ECVC consumes lower bit-rates and the reconstruction frame achieves 1 dB improvements in PSNR. In terms of subjective quality, our ECVC has significant improvements compared to previous SOTA methods, such as DCVC-DC and DCVC-FM.

4.3. Complexity Analysis

We compare the complexity of ECVC with recent DCVC-HEM and DCVC-FM and the baseline DCVC-DC. The results are presented in Table 5. Since the ECVC is based on DCVC-DC with the involvement of MNLC, the complexity of ECVC is slightly higher than that of DCVC-DC. Considering the rate-distortion performance advancement of ECVC over DCVC-DC, the introduction of MNLC is worthwhile.

4.4. Ablation Studies

In ablation studies, all models are optimized with MSE, and PSNR is adopted to evaluate distortion. Table 6 presents the improvements of each component under IP 32 and IP -1 with 96 frames setting. “Base” is our reproduced baseline DCVC-DC*. “Base Large” has 60M params by proportionally increasing all channel dimensions. “LNC” denotes only one reference frame for local and non-local context mining (meaning Base + one reference frame non-local context).

Under IP 32 LNC is able to capture non-local correla-

Method	Venue	BD-Rate (%) w.r.t. VTM-13.2 LDB [8]						Average
		HEVC B	HEVC C	HEVC D	HEVC E	UVG [40]	MCL-JCV [55]	
DCVC-TCM [48]	TMM'22	−20.5	−21.7	−36.2	−20.5	−6.0	−18.6	−20.6
DCVC-HEM [27]	ACMMM'22	−47.4	−43.3	−55.5	−52.4	−32.7	−44.0	−45.9
DCVC-DC [28]	CVPR'23	−53.0	−54.6	−63.4	−60.7	−36.7	−49.1	−52.9
ECVC	Ours	−57.7	−58.2	−65.6	−60.5	−42.7	−54.9	−56.6

¹ The MS-SSIM [56] optimized weights of DCVC-FM are not open-sourced.

Table 2. BD-Rate (%) [5] comparison for MS-SSIM [56]. The anchor is **VTM-13.2 LDB**. The intra period is 32 with 96 frames.

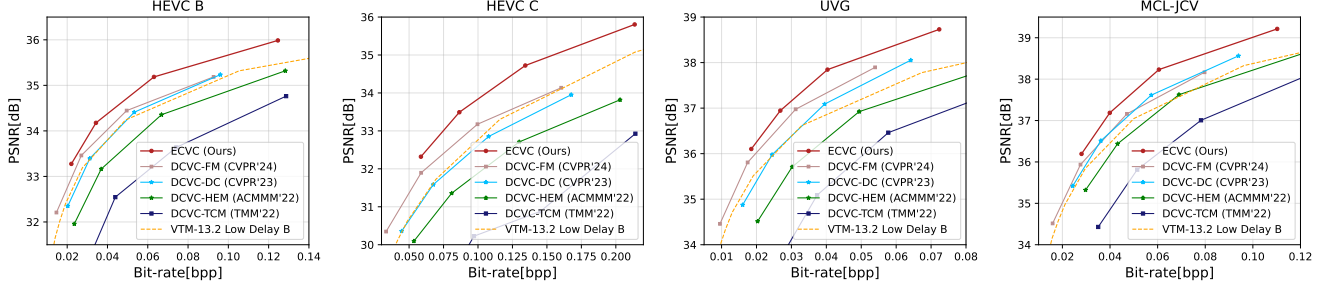


Figure 7. Rate-Distortion curves on HEVC B, HEVC C, UVG and MCL-JCV dataset. **The intra period is −1 with All Frames.**

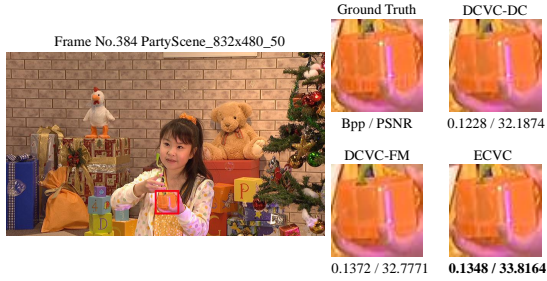


Figure 8. Subjective quality comparison on reconstruction frames of DCVC-DC [28], DCVC-FM [29], the proposed ECVC, and the ground truth.

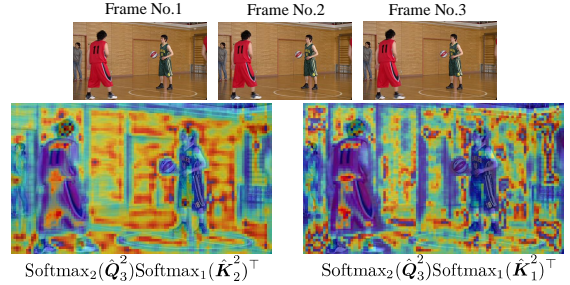


Figure 9. Visualization of non-local correlations. The inputs are the first 3 frames in “BasketballPass_416x240_50”.

tions, which effectively improves the rate-distortion performance. Compared with LNC, the MNLC adopts one more reference frame, enhancing the performance. Thanks to the proposed PCFS, the mismatch of frames between training and inference can be alleviated. The error accumulation is reduced and the performance is further improved.

Under IP −1 Under a long prediction chain, the influence of PCFS is more significant, due to the impacts of error accumulation. Specifically, when equipped with PCFS, the model reduces 45.1% bit-rate over the baseline on HEVC E. Our proposed PCFS is able to finetune the model on *much longer* sequences, thereby reducing accumulated errors.

Visualization of captured non-local correlations To demonstrate the effectiveness of the proposed MNLC in capturing non-local correlations, we visualize its attention maps in Figure 9. For each visualization, we select a query

and compute its attention scores with all keys. Redder colors indicate higher attention scores. It is obvious the MNLC captures the non-local contexts between walls and floors (the texture of walls and floors are similar). The captured non-local contexts are employed as priors for conditional encoding, thereby saving the bit-rate for inter coding.

Influences of finetuning frames With the proposed PCFS, the model can be finetuned with long sequences under limited computational resources. To further analyze the PCFS, we compare the performance of fine-tuning with sequences of different lengths. The results are reported in Table 7. The frame numbers are {6, 20, 38, 55} with {1, 1, 2, 3} groups, respectively. When involving more frames for finetuning, the performance is further improved under both IP −1 and IP 32 scenarios. Notably, for sequences with smaller movements (HEVC E [7]), the gain of using more frames for fine-tuning is substantial. The perfor-

Method	Venue	BD-Rate (%) w.r.t. VTM-13.2 LDB [8]						Average
		HEVC B	HEVC C	HEVC D	HEVC E	UVG [40]	MCL-JCV [55]	
DCVC-TCM [48]	TMM'22	+55.4	+97.4	+50.0	+214.2	+60.4	+50.7	+88.0
DCVC-HEM [27]	ACMMM'22	+3.9	+28.4	−1.2	+66.3	+0.5	+1.7	+16.6
DCVC-DC [28]	CVPR'23	−11.0	+0.2	−23.9	−7.8	−21.0	−13.0	−12.8
DCVC-FM [29]	CVPR'24	−11.7	−7.9	−28.2	−25.8	−23.9	−12.3	−18.3
ECVC	Ours	−27.9	−18.9	−39.0	−26.4	−38.3	−27.7	−29.7

Table 3. BD-Rate (%) [5] comparison for PSNR (dB). The anchor is **VTM-13.2 LDB**. The Intra Period is **−1** with **96** frames.

Method	Venue	BD-Rate (%) w.r.t. VTM-13.2 LDB [8]						Average
		HEVC B	HEVC C	HEVC D	HEVC E	UVG	MCL-JCV	
DCVC-TCM [48]	TMM'22	+107.3	+143.5	+99.2	+835.9	+120.6	+63.7	+228.4
DCVC-HEM [27]	ACMMM'22	+22.8	+32.3	+13.4	+236.9	+33.5	+6.7	+57.6
DCVC-DC [28]	CVPR'23	−7.5	+3.4	−12.0	+83.9	−4.5	−12.9	+8.4
DCVC-FM [29]	CVPR'24	−19.9	−17.4	−25.7	−24.5	−22.5	−13.4	−20.6
ECVC	Ours	−33.4	−29.5	−38.8	−23.5	−37.5	−29.7	−32.1

Table 4. BD-Rate (%) [5] comparison for PSNR (dB). The anchor is **VTM-13.2 LDB**. The Intra Period is **−1** with **All** frames.

Method	Params (M)	kMACs/pixel	ET(s)	DT(s)
DCVC-HEM [27]	50.9	1581	0.67	0.52
DCVC-DC [28]	50.8	1274	0.74	0.59
DCVC-FM [29]	44.9	1073	0.73	0.60
ECVC	61.9	1407	0.78	0.62

Table 5. Complexity comparison among proposed ECVC, DCVC-HEM, DCVC-DC, and DCVC-FM. “Params” denotes the number of model parameters. “kMACs/pixel” denotes the multiply-add operations per pixel on 1080p sequences. “ET”, “DT” are average encoding and decoding time per frame.

Methods	IP	B	C	D	E	Avg
Base (DCVC-DC) Large	32	−2.1	−4.2	−5.4	−0.2	−3.0
Base + MNLC	32	−4.0	−9.9	−9.0	−9.7	−8.2
Base (DCVC-DC) Large	−1	−1.4	−2.4	−4.3	−4.7	−3.2
Base + MNLC	−1	−2.5	−6.5	−7.9	−16.9	−8.5
DCVC-HEM	32	23.1	23.3	26.0	22.9	23.8
DCVC-HEM + PCFS	32	14.1	10.6	14.5	18.7	14.5
Base (DCVC-DC) + PCFS	32	−1.9	−8.5	−8.6	−8.0	−6.8
Base + PCFS + NLC	32	−4.6	−13.0	−12.1	−11.4	−10.3
Base + PCFS + MNLC	32	−9.1	−15.3	−14.5	−14.8	−13.4
DCVC-HEM	−1	29.8	30.8	32.9	18.1	27.9
DCVC-HEM + PCFS	−1	9.8	5.9	9.7	−7.4	4.5
Base (DCVC-DC) + PCFS	−1	−6.0	−11.8	−13.2	−19.4	−12.6
Base + PCFS + NLC	−1	−10.4	−18.5	−19.5	−27.4	−19.0
Base + PCFS + MNLC	−1	−18.1	−25.7	−24.8	−45.1	−28.4

Table 6. Ablation Studies on HEVC B, C, D, E. The anchor is the base model. “IP” denotes the intra period.

mance improvements under both IP −1 and IP 32 settings as the frame number increases can be attributed to the diverse error patterns encountered during fine-tuning, which

Frames	IP	B	C	D	E
6	32	−4.0	−9.9	−9.0	−9.7
20	32	−8.6	−14.5	−12.4	−12.1
38	32	−8.9	−15.0	−14.4	−13.8
55	32	−9.1	−15.3	−14.5	−14.8
6	−1	−0.4	−2.9	−6.7	−9.5
20	−1	−17.1	−24.4	−22.3	−41.3
38	−1	−18.1	−25.7	−24.2	−42.5
55	−1	−18.8	−26.1	−24.8	−45.1

Table 7. Influences of finetuning frames. The anchor is the base model. “IP” denotes the intra period.

enhance ECVC’s generalization capability.

5. Conclusion

In this paper, we demonstrate the effectiveness of exploiting non-local correlations for learned video compression. To extract more temporal priors from multiple frames, we propose the Multiple Frame Non-Local Context Mining approach. The offset diversity, successive flow warping and multi-scale refinement are employed to capture local correlations across multiple frames, while multi-head linear cross attention is employed to capture non-local correlations among them. To reduce the temporal error accumulation, we introduce the partial cascaded finetuning strategy to optimize the model under limited resources. However, while ECVC achieves SOTA performance, it may perform worse than VTM on out-of-domain sequences (*e.g.*, anime videos) because ECVC is trained on natural videos [37, 59]. To address this issue, we will investigate the instance-adaptive optimization techniques [34, 51, 52, 58] in the future.

References

- [1] Eirikur Agustsson, David Minnen, Nick Johnston, Johannes Balle, Sung Jin Hwang, and George Toderici. Scale-space flow for end-to-end optimized video compression. In *Proceedings of the IEEE/CVF Conference on Computer Vision and Pattern Recognition*, pages 8503–8512, 2020. 2
- [2] David Alexandre, Hsueh-Ming Hang, and Wen-Hsiao Peng. Hierarchical b-frame video coding using two-layer canf without motion coding. In *Proceedings of the IEEE/CVF Conference on Computer Vision and Pattern Recognition*, pages 10249–10258, 2023. 1
- [3] Johannes Ballé, Valero Laparra, and Eero P Simoncelli. End-to-end optimized image compression. In *International Conference on Learning Representations*, 2017. 1
- [4] Johannes Ballé, David Minnen, Saurabh Singh, Sung Jin Hwang, and Nick Johnston. Variational image compression with a scale hyperprior. In *International Conference on Learning Representations*, 2018. 1
- [5] Gisle Bjontegaard. Calculation of average psnr differences between rd-curves. *ITU-T SG16 Q*, 6, 2001. 6, 7, 8, 13, 14
- [6] Frank Bossen, Jill Boyce, Xiang Li, Vadim Seregin, and Karsten Sühling. Jvet common test conditions and software reference configurations for sdr video. *Joint Video Experts Team (JVET) of ITU-T SG*, 16:19–27, 2019. 6
- [7] Frank Bossen et al. Common test conditions and software reference configurations. *JCTVC-L1100*, 12(7):1, 2013. 5, 7
- [8] Benjamin Bross, Ye-Kui Wang, Yan Ye, Shan Liu, Jianle Chen, Gary J Sullivan, and Jens-Rainer Ohm. Overview of the versatile video coding (vvc) standard and its applications. *IEEE Transactions on Circuits and Systems for Video Technology*, 31(10):3736–3764, 2021. 1, 6, 7, 8, 12, 13, 14
- [9] Kelvin CK Chan, Xintao Wang, Ke Yu, Chao Dong, and Chen Change Loy. Understanding deformable alignment in video super-resolution. In *Proceedings of the AAAI conference on artificial intelligence*, pages 973–981, 2021. 2
- [10] Mu-Jung Chen, Yi-Hsin Chen, and Wen-Hsiao Peng. B-canf: Adaptive b-frame coding with conditional augmented normalizing flows. *IEEE Transactions on Circuits and Systems for Video Technology*, 34(4):2908–2921, 2024. 1
- [11] Yi-Hsin Chen, Hong-Sheng Xie, Cheng-Wei Chen, Zong-Lin Gao, Martin Benjak, Wen-Hsiao Peng, and Jörn Ostermann. Maskcrt: Masked conditional residual transformer for learned video compression. *IEEE Transactions on Circuits and Systems for Video Technology*, 2024. 1
- [12] Jifeng Dai, Haozhi Qi, Yuwen Xiong, Yi Li, Guodong Zhang, Han Hu, and Yichen Wei. Deformable convolutional networks. In *Proceedings of the IEEE International Conference on Computer Vision*, pages 764–773, 2017. 2
- [13] Rui Fan, Yongfei Zhang, and Bo Li. Motion classification-based fast motion estimation for high-efficiency video coding. *IEEE Transactions on Multimedia*, 19(5):893–907, 2016. 3
- [14] Haifeng Guo, Sam Kwong, Dongjie Ye, and Shiqi Wang. Enhanced context mining and filtering for learned video compression. *IEEE Transactions on Multimedia*, 2023. 1
- [15] Zongyu Guo, Runsen Feng, Zhizheng Zhang, Xin Jin, and Zhibo Chen. Learning cross-scale weighted prediction for efficient neural video compression. *IEEE Transactions on Image Processing*, 32:3567–3579, 2023. 1
- [16] Dongchen Han, Xuran Pan, Yizeng Han, Shiji Song, and Gao Huang. Flatten transformer: Vision transformer using focused linear attention. In *Proceedings of the IEEE/CVF international conference on computer vision*, pages 5961–5971, 2023. 4
- [17] Yung-Han Ho, Chih-Peng Chang, Peng-Yu Chen, Alessandro Gnutti, and Wen-Hsiao Peng. Canf-vc: Conditional augmented normalizing flows for video compression. In *Proceedings of the European Conference on Computer Vision*, pages 207–223. Springer, 2022. 1
- [18] Zhihao Hu, Zhenghao Chen, Dong Xu, Guo Lu, Wanli Ouyang, and Shuhang Gu. Improving deep video compression by resolution-adaptive flow coding. In *Proceedings of the European Conference on Computer Vision*, pages 193–209. Springer, 2020. 2
- [19] Zhihao Hu, Guo Lu, and Dong Xu. Fvc: A new framework towards deep video compression in feature space. In *Proceedings of the IEEE/CVF Conference on Computer Vision and Pattern Recognition*, pages 1502–1511, 2021. 1, 2
- [20] Zhihao Hu, Guo Lu, Jinyang Guo, Shan Liu, Wei Jiang, and Dong Xu. Coarse-to-fine deep video coding with hyperprior-guided mode prediction. In *Proceedings of the IEEE/CVF Conference on Computer Vision and Pattern Recognition*, pages 5921–5930, 2022. 2
- [21] Yu-Wen Huang, Bing-Yu Hsieh, Shao-Yi Chien, Shyh-Yih Ma, and Liang-Gee Chen. Analysis and complexity reduction of multiple reference frames motion estimation in h. 264/avc. *IEEE Transactions on Circuits and Systems for Video Technology*, 16(4):507–522, 2006. 2, 3
- [22] Wei Jiang and Ronggang Wang. Mlic++: Linear complexity multi-reference entropy modeling for learned image compression. In *ICML 2023 Workshop Neural Compression: From Information Theory to Applications*, 2023. 4
- [23] Wei Jiang, Jiayu Yang, Yongqi Zhai, Peirong Ning, Feng Gao, and Ronggang Wang. Mlic: Multi-reference entropy model for learned image compression. In *Proceedings of the 31st ACM International Conference on Multimedia*, pages 7618–7627, 2023. 4
- [24] Wei Jiang, Junru Li, Kai Zhang, and Li Zhang. Lvc-lgmc: Joint local and global motion compensation for learned video compression. In *IEEE International Conference on Acoustics, Speech and Signal Processing*, pages 2955–2959. IEEE, 2024. 1
- [25] Angelos Katharopoulos, Apoorv Vyas, Nikolaos Pappas, and François Fleuret. Transformers are rnns: Fast autoregressive transformers with linear attention. In *International Conference on Machine Learning*, pages 5156–5165. PMLR, 2020. 4
- [26] Jiahao Li, Bin Li, and Yan Lu. Deep contextual video compression. *Advances in Neural Information Processing Systems*, 34:18114–18125, 2021. 1, 2, 5
- [27] Jiahao Li, Bin Li, and Yan Lu. Hybrid spatial-temporal entropy modelling for neural video compression. In *Proceedings of the 30th ACM International Conference on Multimedia*, pages 1503–1511, 2022. 1, 3, 5, 6, 7, 8, 13, 14

- [28] Jiahao Li, Bin Li, and Yan Lu. Neural video compression with diverse contexts. In *Proceedings of the IEEE/CVF Conference on Computer Vision and Pattern Recognition*, pages 22616–22626, 2023. 1, 2, 3, 5, 6, 7, 8, 12, 13, 14
- [29] Jiahao Li, Bin Li, and Yan Lu. Neural video compression with feature modulation. In *Proceedings of the IEEE/CVF Conference on Computer Vision and Pattern Recognition*, pages 26099–26108, 2024. 1, 2, 3, 5, 6, 7, 8, 12, 13, 14
- [30] Kai Lin, Chuanmin Jia, Xinfeng Zhang, Shanshe Wang, Siwei Ma, and Wen Gao. Dmvc: Decomposed motion modeling for learned video compression. *IEEE Transactions on Circuits and Systems for Video Technology*, 33(7):3502–3515, 2023. 1
- [31] Bowen Liu, Yu Chen, Rakesh Chowdary Machineni, Shiyu Liu, and Hun-Seok Kim. Mmvc: Learned multi-mode video compression with block-based prediction mode selection and density-adaptive entropy coding. In *Proceedings of the IEEE/CVF Conference on Computer Vision and Pattern Recognition*, pages 18487–18496, 2023. 5
- [32] Haojie Liu, Han Shen, Lichao Huang, Ming Lu, Tong Chen, and Zhan Ma. Learned video compression via joint spatial-temporal correlation exploration. In *Proceedings of the AAAI Conference on Artificial Intelligence*, pages 11580–11587, 2020. 1
- [33] Guo Lu, Wanli Ouyang, Dong Xu, Xiaoyun Zhang, Chunlei Cai, and Zhiyong Gao. Dvc: An end-to-end deep video compression framework. In *Proceedings of the IEEE/CVF Conference on Computer Vision and Pattern Recognition*, pages 11006–11015, 2019. 1, 2, 5
- [34] Guo Lu, Chunlei Cai, Xiaoyun Zhang, Li Chen, Wanli Ouyang, Dong Xu, and Zhiyong Gao. Content adaptive and error propagation aware deep video compression. In *Proceedings of the European Conference on Computer Vision*, pages 456–472. Springer, 2020. 5, 8
- [35] Guo Lu, Xiaoyun Zhang, Wanli Ouyang, Li Chen, Zhiyong Gao, and Dong Xu. An end-to-end learning framework for video compression. *IEEE transactions on pattern analysis and machine intelligence*, 43(10):3292–3308, 2020. 1
- [36] Ming Lu, Zhihao Duan, Fengqing Zhu, and Zhan Ma. Deep hierarchical video compression. In *Proceedings of the AAAI Conference on Artificial Intelligence*, pages 8859–8867, 2024. 1, 5
- [37] Di Ma, Fan Zhang, and David R Bull. Bvi-dvc: A training database for deep video compression. *IEEE Transactions on Multimedia*, 24:3847–3858, 2021. 5, 8
- [38] Siwei Ma, Xinfeng Zhang, Chuanmin Jia, Zhenghui Zhao, Shiqi Wang, and Shanshe Wang. Image and video compression with neural networks: A review. *IEEE Transactions on Circuits and Systems for Video Technology*, 30(6):1683–1698, 2019. 1
- [39] Fabian Mentzer, George D Toderici, David Minnen, Sergi Caelles, Sung Jin Hwang, Mario Lucic, and Eirikur Agustsson. Vct: A video compression transformer. *Advances in Neural Information Processing Systems*, 35:13091–13103, 2022. 1
- [40] Alexandre Mercat, Marko Viitanen, and Jarno Vanne. Uvg dataset: 50/120fps 4k sequences for video codec analysis and development. In *Proceedings of the 11th ACM Multimedia Systems Conference*, pages 297–302, 2020. 1, 6, 7, 8, 13, 14
- [41] Adam Paszke, Sam Gross, Francisco Massa, Adam Lerer, James Bradbury, Gregory Chanan, Trevor Killeen, Zeming Lin, Natalia Gimelshein, Luca Antiga, et al. Pytorch: An imperative style, high-performance deep learning library. *Advances in neural information processing systems*, 32, 2019. 5
- [42] Reza Pourreza and Taco Cohen. Extending neural p-frame codecs for b-frame coding. In *Proceedings of the IEEE/CVF International Conference on Computer Vision*, pages 6680–6689, 2021. 1
- [43] Reza Pourreza, Hoang Le, Amir Said, Guillaume Sautiere, and Auke Wiggers. Boosting neural video codecs by exploiting hierarchical redundancy. In *Proceedings of the IEEE/CVF Winter Conference on Applications of Computer Vision*, pages 5355–5364, 2023. 1
- [44] Linfeng Qi, Jiahao Li, Bin Li, Houqiang Li, and Yan Lu. Motion information propagation for neural video compression. In *Proceedings of the IEEE/CVF Conference on Computer Vision and Pattern Recognition*, pages 6111–6120, 2023. 1
- [45] Anurag Ranjan and Michael J Black. Optical flow estimation using a spatial pyramid network. In *Proceedings of the IEEE/CVF conference on computer vision and pattern recognition*, pages 4161–4170, 2017. 2
- [46] Oren Rippel, Alexander G Anderson, Kedar Tatwawadi, Sanjay Nair, Craig Lytle, and Lubomir Bourdev. Elf-vc: Efficient learned flexible-rate video coding. In *Proceedings of the IEEE/CVF International Conference on Computer Vision*, pages 14479–14488, 2021. 1
- [47] Zhuoran Shen, Mingyuan Zhang, Haiyu Zhao, Shuai Yi, and Hongsheng Li. Efficient attention: Attention with linear complexities. In *Proceedings of the IEEE/CVF Winter Conference on Applications of Computer Vision*, pages 3531–3539, 2021. 4
- [48] Xihua Sheng, Jiahao Li, Bin Li, Li Li, Dong Liu, and Yan Lu. Temporal context mining for learned video compression. *IEEE Transactions on Multimedia*, 25:7311–7322, 2022. 1, 3, 5, 6, 7, 8, 13, 14
- [49] Xihua Sheng, Li Li, Dong Liu, and Houqiang Li. Spatial decomposition and temporal fusion based inter prediction for learned video compression. *IEEE Transactions on Circuits and Systems for Video Technology*, 34(7):6460–6473, 2024. 1, 5
- [50] Yibo Shi, Yunying Ge, Jing Wang, and Jue Mao. Alphavc: High-performance and efficient learned video compression. In *Proceedings of the European Conference on Computer Vision*, pages 616–631. Springer, 2022. 2
- [51] Chuanbo Tang, Xihua Sheng, Zhuoyuan Li, Haotian Zhang, Li Li, and Dong Liu. Offline and online optical flow enhancement for deep video compression. In *Proceedings of the AAAI Conference on Artificial Intelligence*, pages 5118–5126, 2024. 8
- [52] Ties van Rozendaal, Johann Brehmer, Yunfan Zhang, Reza Pourreza, Auke J Wiggers, and Taco Cohen. Instance-adaptive video compression: Improving neural codecs by training on the test set. *Transactions on Machine Learning Research*, 2023. 8

- [53] Ashish Vaswani, Noam Shazeer, Niki Parmar, Jakob Uszkoreit, Llion Jones, Aidan N Gomez, Łukasz Kaiser, and Illia Polosukhin. Attention is all you need. *Advances in neural information processing systems*, 30, 2017. [2](#)
- [54] Huairui Wang and Zhenzhong Chen. Exploring long- and short-range temporal information for learned video compression. *IEEE Transactions on Image Processing*, 33:780–792, 2024. [1](#)
- [55] Haiqiang Wang, Weihao Gan, Sudeng Hu, Joe Yuchieh Lin, Lina Jin, Longguang Song, Ping Wang, Ioannis Katsavounidis, Anne Aaron, and C-C Jay Kuo. Mcl-jcv: a jnd-based h. 264/avc video quality assessment dataset. In *IEEE International Conference on Image Processing*, pages 1509–1513. IEEE, 2016. [6](#), [7](#), [8](#), [13](#), [14](#)
- [56] Zhou Wang, Eero P Simoncelli, and Alan C Bovik. Multiscale structural similarity for image quality assessment. In *The Thirty-Seventh Asilomar Conference on Signals, Systems & Computers, 2003*, pages 1398–1402. IEEE, 2003. [5](#), [6](#), [7](#), [13](#)
- [57] Jinxi Xiang, Kuan Tian, and Jun Zhang. Mimt: Masked image modeling transformer for video compression. In *International Conference on Learning Representations*, 2023. [1](#)
- [58] Tongda Xu, Han Gao, Chenjian Gao, Yuanyuan Wang, Dailan He, Jinyong Pi, Jixiang Luo, Ziyu Zhu, Mao Ye, Hongwei Qin, et al. Bit allocation using optimization. In *International Conference on Machine Learning*, pages 38377–38399. PMLR, 2023. [8](#)
- [59] Tianfan Xue, Baian Chen, Jiajun Wu, Donglai Wei, and William T Freeman. Video enhancement with task-oriented flow. *International Journal of Computer Vision*, 127(8): 1106–1125, 2019. [5](#), [8](#)
- [60] Jiayu Yang, Wei Jiang, Yongqi Zhai, Chunhui Yang, and Ronggang Wang. Ucvc: A unified contextual video compression framework with joint p-frame and b-frame coding. In *Proceedings of the Data Compression Conference*, pages 382–391. IEEE, 2024. [1](#)
- [61] Jiayu Yang, Yongqi Zhai, Wei Jiang, Chunhui Yang, Feng Gao, and Ronggang Wang. Adaptive prediction structure for learned video compression. *ACM Transactions on Multimedia Computing, Communications and Applications*, 21(2):1–23, 2024. [1](#)
- [62] Ren Yang, Fabian Mentzer, Luc Van Gool, and Radu Timofte. Learning for video compression with hierarchical quality and recurrent enhancement. In *Proceedings of the IEEE/CVF Conference on Computer Vision and Pattern Recognition*, pages 6628–6637, 2020.
- [63] Ruihan Yang, Yibo Yang, Joseph Marino, and Stephan Mandt. Insights from generative modeling for neural video compression. *IEEE Transactions on Pattern Analysis and Machine Intelligence*, 45(8):9908–9921, 2023. [1](#)
- [64] Yibo Yang, Stephan Mandt, Lucas Theis, et al. An introduction to neural data compression. *Foundations and Trends® in Computer Graphics and Vision*, 15(2):113–200, 2023. [1](#)
- [65] Yongqi Zhai, Jiayu Yang, Wei Jiang, Chunhui Yang, Luyang Tang, and Ronggang Wang. Hybrid local-global context learning for neural video compression. In *Proceedings of the Data Compression Conference*, pages 322–331. IEEE, 2024. [1](#)
- [66] Kai Zhang, Yi-Wen Chen, Li Zhang, Wei-Jung Chien, and Marta Karczewicz. An improved framework of affine motion compensation in video coding. *IEEE Transactions on Image Processing*, 28(3):1456–1469, 2018. [3](#)

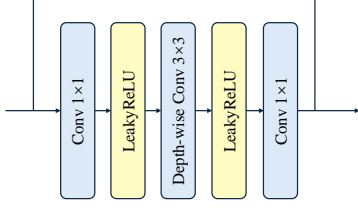


Figure 10. Architecture of the depth-wise Res Block.

A. Network Structure

Our ECVC is based on DCVC-DC [28], but focuses more on exploiting non-local correlations in multiple frames to boost the rate-distortion performance. Here we describe implementation details in the introduced components to DCVC-DC.

A.1. Embedding Layers and Depth-wise Res Block

In the multi-head linear cross attention layer, the depth-wise res block are employed for embedding and point-wise interactions. The structure of the depth-wise res block is depicted in Figure 10.

A.2. Multi-Scale Refine Module

The architecture of multi-scale refine module is depicted in Figure 11.

A.3. Channel numbers

The channel numbers of multi-scale features are $\{d_f^0, d_f^1, d_f^2\} = \{48, 64, 96\}$.

The channel numbers of mid-features during encoding are $\{d_e^0, d_e^1, d_e^2\} = \{3, 64, 96\}$.

The channel numbers of mid-features during decoding are $\{d_d^0, d_d^1, d_d^2\} = \{32, 64, 96\}$.

B. ECVC-FM

We introduce ECVC-FM, a new variant of ECVC that adopts DCVC-FM [29] as its backbone while incorporating key techniques from ECVC. Additionally, we modify the channel dimensions of temporal contexts, resulting in a model with 53.05M parameters.

C. Test Settings

To conduct comparisons, we compare the LVCs and traditional codecs in both RGB color space. BT.601 is employed to convert the frames in YUV color space to RGB color space. To obtain the RD data of VTM-13.2 LDB [8], following commands are employed:

```
EncoderApp
-c encoder_lowdelay_vtm.cfg
--InputFile={input file name}
--BitstreamFile={bitstream file name}
--DecodingRefreshType=2
--InputBitDepth=8
--OutputBitDepth=8
--OutputBitDepthC=8
--InputChromaFormat=444
--FrameRate={frame rate}
--FramesToBeEncoded={frame number}
--SourceWidth={width}
--SourceHeight={height}
--IntraPeriod={IP}
--QP={qp}
--Level=6.2
```

For DCVC-DC and DCVC-FM [29], we use the official weights and code to evaluate the performance.

D. Rate-Distortion Results

We provide the performances of our baseline model, reproduced DCVC-DC* in Table 8, Table 9, Table 10 and Table 11. The bpp-PSNR curves are presented in Figure 12, Figure 13 and Figure 14. The bpp-MS-SSIM curves are presented in Figure 15.

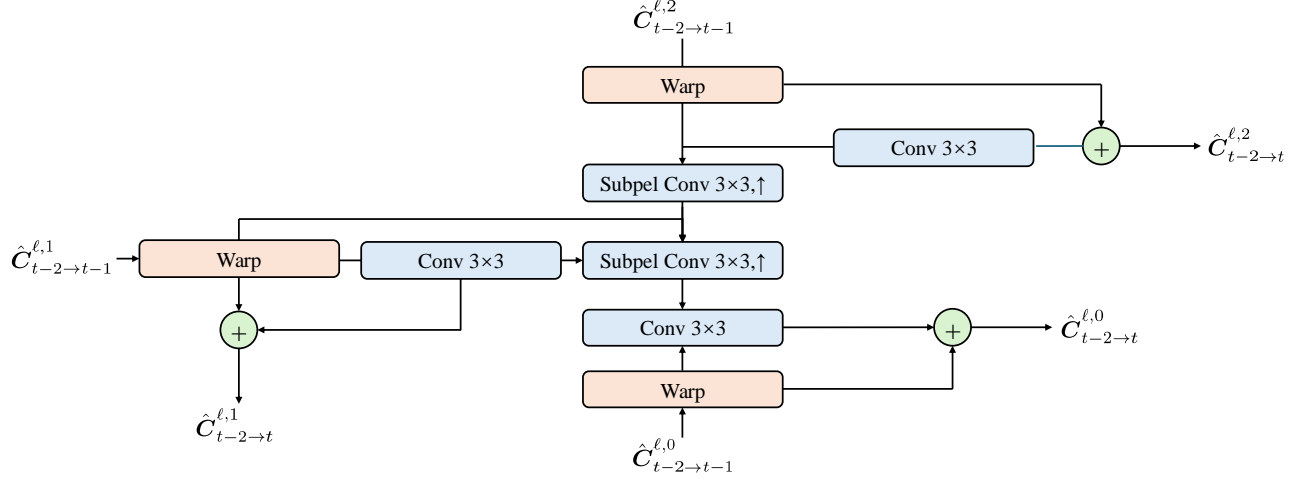


Figure 11. Architecture of multi-scale refine module. “Subpel Conv” means sub pixel convolution.

Method	Venue	BD-Rate (%) w.r.t. VTM-13.2 LDB [8]						Average
		HEVC B	HEVC C	HEVC D	HEVC E	UVG [40]	MCL-JCV [55]	
DCVC-TCM [48]	TMM’22	+28.5	+60.5	+27.8	+67.3	+17.1	+30.6	+38.6
DCVC-HEM [27]	ACMMM’22	−5.1	+15.0	−8.9	+7.1	−18.2	−6.4	−2.8
DCVC-DC [28]	CVPR’23	−17.4	−9.8	−29.0	−26.0	−30.0	−20.0	−22.0
DCVC-FM [29]	CVPR’24	−12.5	−10.3	−26.5	−26.9	−24.0	−12.7	−18.8
DCVC-DC*	Reproduced	−20.5	−6.8	−27.1	−12.1	−29.0	−19.3	−19.1
ECVC	Ours	−28.3	−19.6	−36.7	−27.1	−37.6	−26.3	−29.3
ECVC-FM	Ours	−30.9	−22.9	−40.7	−23.4	−42.5	−33.6	−32.3

¹ The quality indexes of DCVC-FM are set to match the bit-rate range of DCVC-DC.

² Please note that the ECVC is based on our reproduced DCVC-DC* since training scripts of DCVC series are not open-sourced.

Table 8. BD-Rate (%) [5] comparison for PSNR (dB). The anchor is **VTM-13.2 LDB. The Intra Period is 32 with 96 frames.**

Method	Venue	BD-Rate (%) w.r.t. VTM-13.2 LDB [8]						Average
		HEVC B	HEVC C	HEVC D	HEVC E	UVG [40]	MCL-JCV [55]	
DCVC-TCM [48]	TMM’22	−20.5	−21.7	−36.2	−20.5	−6.0	−18.6	−20.6
DCVC-HEM [27]	ACMMM’22	−47.4	−43.3	−55.5	−52.4	−32.7	−44.0	−45.9
DCVC-DC [28]	CVPR’23	−53.0	−54.6	−63.4	−60.7	−36.7	−49.1	−52.9
DCVC-DC*	Reproduced	−53.5	−52.8	−61.6	−48.8	−39.1	−52.2	−51.3
ECVC	Ours	−57.7	−58.2	−65.6	−60.5	−42.7	−54.9	−56.6

¹ The MS-SSIM [56] optimized weights of DCVC-FM are not open-sourced.

Table 9. BD-Rate (%) [5] comparison for MS-SSIM [56]. The anchor is **VTM-13.2 LDB. The intra period is 32 with 96 frames.**

Method	Venue	BD-Rate (%) w.r.t. VTM-13.2 LDB [8]						Average
		HEVC B	HEVC C	HEVC D	HEVC E	UVG [40]	MCL-JCV [55]	
DCVC-TCM [48]	TMM'22	+55.4	+97.4	+50.0	+214.2	+60.4	+50.7	+88.0
DCVC-HEM [27]	ACMMM'22	+3.9	+28.4	−1.2	+66.3	+0.5	+1.7	+16.6
DCVC-DC [28]	CVPR'23	−11.0	+0.2	−23.9	−7.8	−21.0	−13.0	−12.8
DCVC-FM [29]	CVPR'24	−11.7	−7.9	−28.2	−25.8	−23.9	−12.3	−18.3
DCVC-DC*	Reproduced	−9.2	+6.9	−20.0	+45.1	−12.5	−11.7	−0.2
ECVC	Ours	−27.9	−18.9	−39.0	−26.4	−38.3	−27.7	−29.7
ECVC-FM	Ours	−30.9	−22.9	−40.7	−23.4	−42.5	−33.6	−32.3

Table 10. BD-Rate (%) [5] comparison for PSNR (dB). The anchor is **VTM-13.2 LDB**. The Intra Period is **−1 with 96 frames**.

Method	Venue	BD-Rate (%) w.r.t. VTM-13.2 LDB [8]						Average
		HEVC B	HEVC C	HEVC D	HEVC E	UVG	MCL-JCV	
DCVC-TCM [48]	TMM'22	+107.3	+143.5	+99.2	+835.9	+120.6	+63.7	+228.4
DCVC-HEM [27]	ACMMM'22	+22.8	+32.3	+13.4	+236.9	+33.5	+6.7	+57.6
DCVC-DC [28]	CVPR'23	−7.5	+3.4	−12.0	+83.9	−4.5	−12.9	+8.4
DCVC-FM [29]	CVPR'24	−19.9	−17.4	−25.7	−24.5	−22.5	−13.4	−20.6
DCVC-DC*	Reproduced	+11.9	+11.6	−3.6	+446.4	+16.2	−9.8	+78.8
ECVC	Ours	−33.4	−29.5	−38.8	−23.5	−37.5	−29.7	−32.1
ECVC-FM	Ours	−33.5	−32.7	−41.3	−17.3	−41.3	−34.3	−33.4

Table 11. BD-Rate (%) [5] comparison for PSNR (dB). The anchor is **VTM-13.2 LDB**. The Intra Period is **−1 with All frames**.

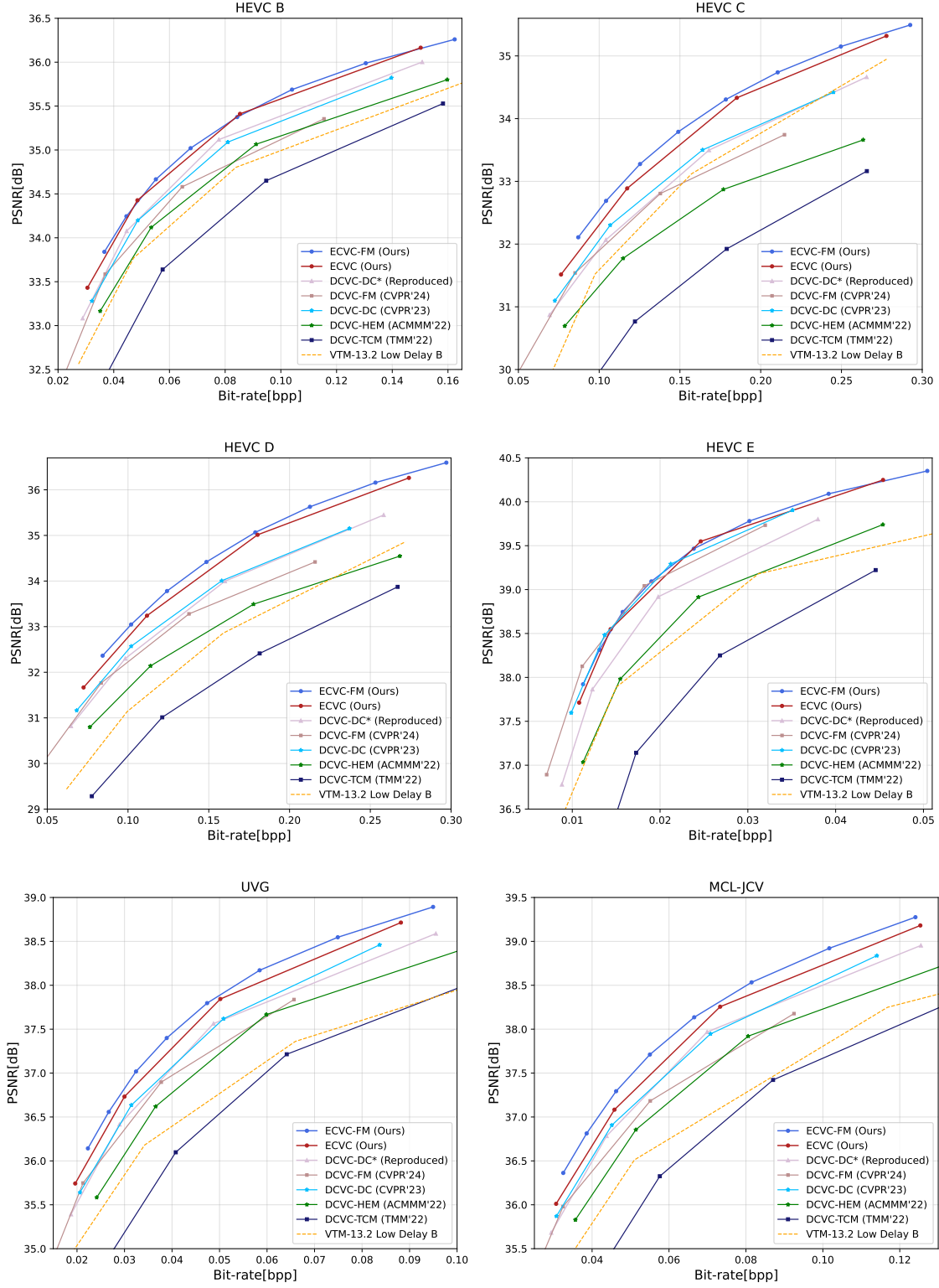


Figure 12. Bpp-PSNR curves on HEVC B, C, D, E, UVG and MCL-JCV dataset. The intra period is 32 with 96 frames.

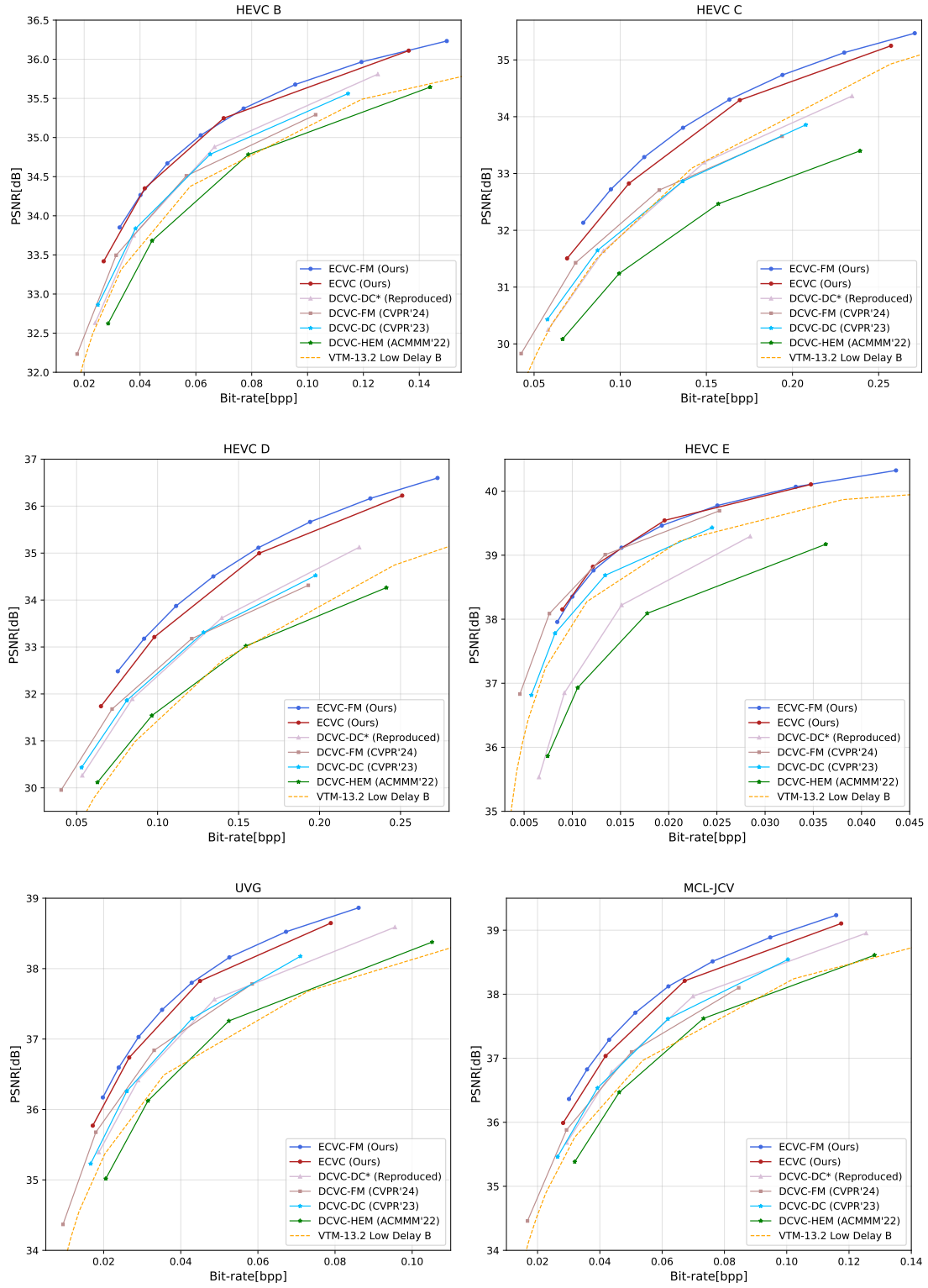


Figure 13. Bpp-PSNR curves on HEVC B, C, D, E, UVG and MCL-JCV dataset. **The intra period is -1 with 96 frames.**

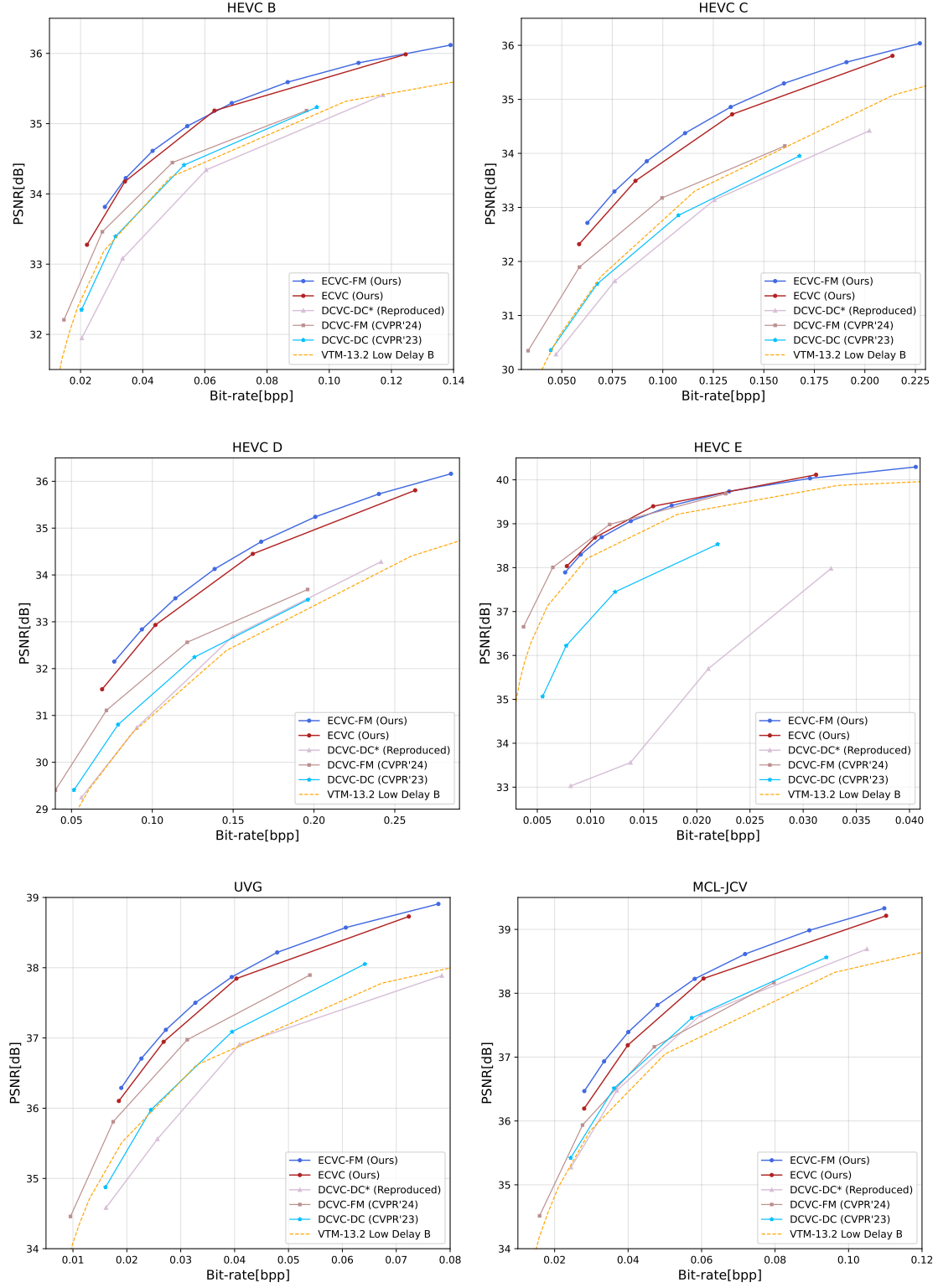


Figure 14. Bpp-PSNR curves on HEVC B, C, D, E, UVG and MCL-JCV dataset. **The intra period is -1 with All frames.**

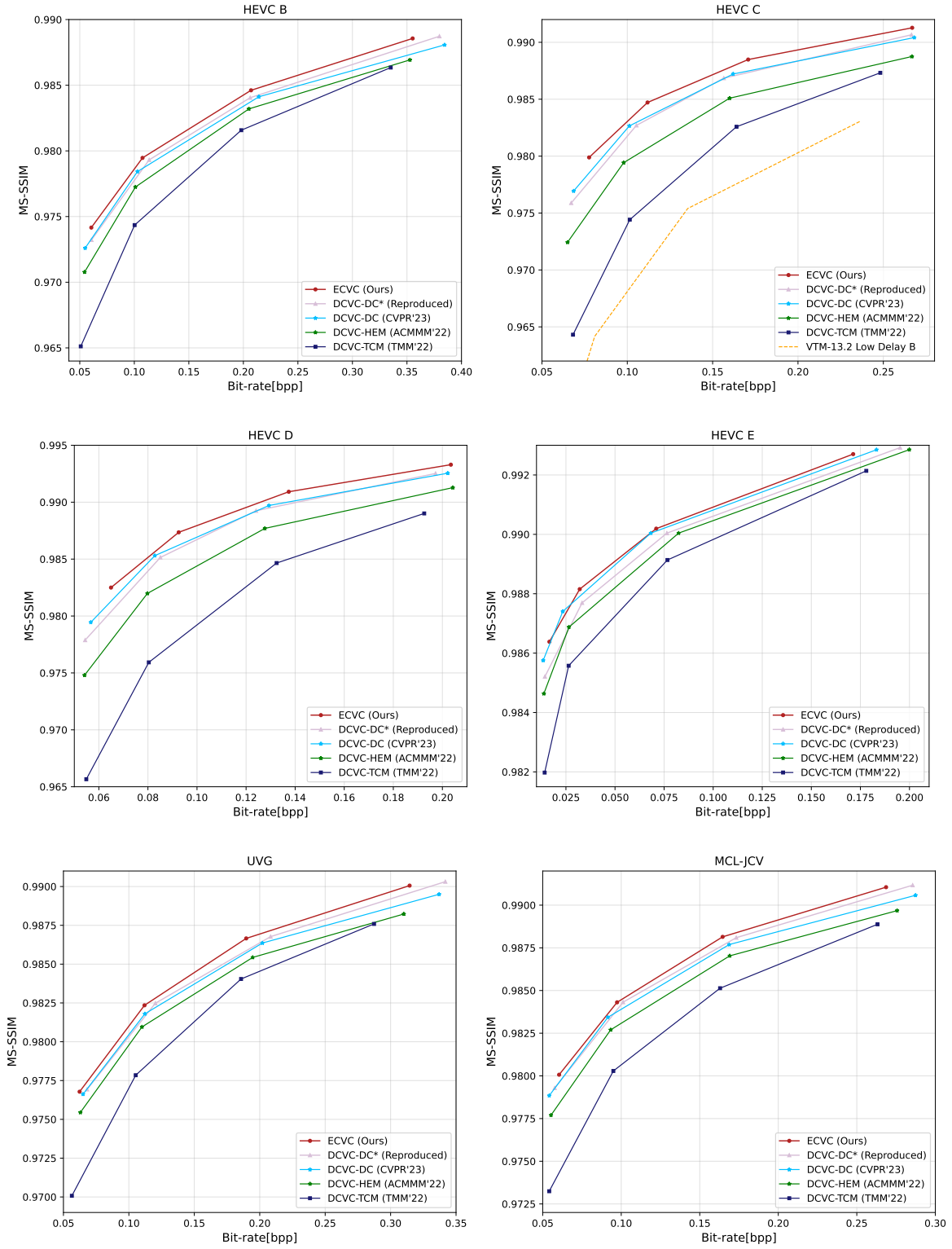


Figure 15. Bpp-MS-SSIM curves on HEVC B, C, D, E, UVG and MCL-JCV dataset. **The intra period is 32 with 96 frames.**